An Analog Hardware Classifier for Estimating Sea State or Wave Height from Inertial Sensor Data

Vassilis Alimisis, Nikolaos P. Eleftheriou, Georgios Georgousis and Paul P. Sotiriadis

Department of Electrical and Computer Engineering
National Technical University of Athens, Greece
E-mail: alimisisv@gmail.com, eleftheriou_nikos@hotmail.com, geordag@otenet.gr, pps@ieee.org

***Abstract*—The related research presents a novel methodology for implementing power-efficient analog classifiers, achieving a power consumption of merely 176nW. These classifiers efficiently process multiple input features while sustaining a high degree of precision and minimizing power consumption. It is based on Threshold Machine Learning model, and integrates sigmoid activation circuit along with current comparators. Validation of the implementation was performed employing a real-time vessel dataset, achieving a good accuracy of 82.95% in predicting true waves from inertial sensor data. Furthermore, a comparative analysis was conducted with other analog classifiers employing the identical dataset. All related models were trained using a software-based equivalent one. The executed design was implemented using a TSMC 90nm CMOS process. It is simulated with the Cadence IC Suite.**

***Index Terms*—Inertial sensor data, analog VLSI design, sea state, wave height, power-efficiency**

I. Introduction

Inertial sensors are vital components within a wide array of technological applications, ranging from aerospace and automotive systems to consumer electronics and wearable devices [1], [2]. These sensors function on the principle of measuring the acceleration, angular velocity, and sometimes orientation of an object relative to an inertial frame of reference [3]. By utilizing accelerometers and gyroscopes, inertial sensors can precisely track changes in velocity and orientation, enabling them to play a pivotal role in tasks such as navigation, motion analysis, and stabilization [4], [5]. Their compact size, low power consumption, and high accuracy have made them indispensable tools in fields like robotics, virtual reality, and even healthcare.

As the degree of autonomy in maritime operations escalates, a concurrent augmentation in the deployment of inertial sensors is observed [6]. Estimating sea state or wave height through the use of inertial sensors represents a pivotal advancement in maritime technology [7]. These sensors, designed to measure the accelerations and angular velocities experienced by a vessel, offer a means to discern crucial information about the prevailing sea conditions [8]. By analyzing the dynamic responses of a vessel to wave-induced motions, valuable insights into wave height, frequency, and direction can be derived [7], [9]. These data not only enhances maritime safety by providing real-time information for vessel operators to navigate through rough seas, but also prove invaluable for various offshore operations, such as oil and gas exploration, where knowledge of wave conditions is paramount [7], [9]. Moreover, the integration of inertial sensors for sea state estimation showcases a remarkable fusion of cutting-edge sensor technology with the imperative needs of the maritime industry, clarifying how innovation continues to drive progress in this vital sector.

Driven by the need for low-power and space-efficient solutions in smart inertial sensors for estimating sea state or wave height [10], [11], this study introduces a power-efficient ($176nW$) and low-voltage (0.6V) analog hardware threshold classifier, incorporating a sigmoid activation function. The implemented classifier represents a promising approach. It is suitable for smart sensor classification systems relying on battery power, as it attains an accuracy of 82.95%. It has been designed and validated using a real measurement dataset supplied by METIS Cyberspace Technology company. The performance of the proposed design is verified through layout related (post-layout) simulation results. They are conducted in a TSMC 90nm CMOS process. The related simulations are extracted utilizing Cadence IC Suite. This validation is accomplished by comparing the results with those obtained from a software-based approach and classifiers related to analog circuits.

The structure of this paper unfolds as follows: Section II delves into the mathematical underpinnings pertinent to the analog integrated threshold classifier proposed in this work. Section III outlines the primary components and the envisaged architecture of the classifier. The validation of the proposed classifier is conducted in Section IV, leveraging a real-world sea state dataset derived from inertial sensors. This section further includes a comparative analysis. More specifically the analog integrated and software implementations are provided, supplemented by sensitivity tests. Section V offers a comparative study and engages in a comprehensive discussion. Finally, in Section VI, we draw concluding remarks that encapsulate the key findings and implications of this study.

II. Sigmoid Threshold Classifier

Threshold classifiers, akin to simplified versions of Support Vector Machines (SVMs), find practical application in scenar-

979-8-3503-1884-5/24/$31.00 ©2024 IEEE

ios where classes do not exhibit inherent linear separability [12]. Through the application of a non-linear transformation function denoted as $\phi()$, these classifiers have the capacity to map the data onto a higher-dimensional feature space, rendering the classes either linearly separable or nearly. Subsequently, a threshold value denoted as I_{th} is adjusted to facilitate effective class differentiation. The decision criterion for the threshold classifier can be summarized as follows:

$$y = \begin{cases} 1 & \text{if } \phi(X) \geq I_{th} \\ 2 & \text{if } \phi(X) < I_{th} \end{cases} . \tag{1}$$

In this context, y represents the classifier's prediction, while $\boldsymbol{X}$ denotes a specific input vector. The simplicity of this architecture lends itself well to hardware implementations, as it efficiently minimizes chip area without sacrificing classification accuracy.

This study employs a mathematical model to represent each sub-class with a single feature, specifically a one-dimensional sigmoid activation function [12]. The model is formulated as a summation of univariate sigmoid activation functions, akin to circuits of sigmoid-based current summation, and can be approximated by:

$$\phi(X) = \sum_{i=1}^{K} \{\phi_i(X)\}. \tag{2}$$

In this specific application, $\phi_i()$ is selected to be a univariate sigmoid activation function, defined by:

$$\phi_i(X) = A \cdot \frac{1}{1 + e^{(-x+\mu_i)}}. \tag{3}$$

where parameter μ and A denote the mean value and amplitude of the sigmoid function. The choice of the sigmoid function is motivated by its ease of implementation compared to other alternatives.

III. Classifier: Architecture and Main Blocks

In this section, we introduce both the architecture and the essential building blocks related to the proposed analog threshold classifier. To achieve this implementation, it requires the use of a sigmoid function circuit [13] and a Winner-Takes-All (WTA) circuit [14]. The entire classifier is designed to function with a supply voltage set at $V_{DD} = -V_{SS} = 0.3V$. Here, we have employed sub-threshold region techniques to reduce power consumption.

Each sigmoid function circuit, illustrated in Fig. 1, serves the purpose of generating a univariate sigmoid function curve. This circuit comprises a PMOS cascode current mirror (consisting of transistors M_{p2},M_{p3} and M_{p5},M_{p6}), a NMOS cascode current mirror (consisting of transistors M_{n3} to M_{n6}) to ensure the production of high quality sigmoid curves, even for small bias currents and a simple differential pair M_{n1}, M_{n2}. Its electronic tuning capability provides precise control over the non-linear transformation function, offering both flexibility and accuracy in its behavior. The related simulation results are provided in Fig. 2. The I_{bias} and V_r parameters tunes the height and the mean value of the sigmoid function respectively. The dimensions of the transistors for a single sigmoid function circuit are summarized in Table I.

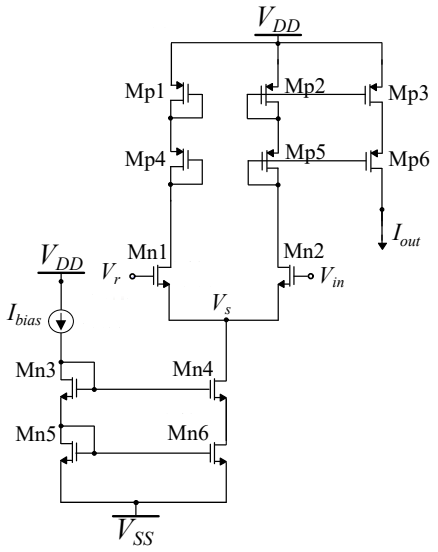

Fig. 1: Here, the design of the sigmoid function circuit. It composed of two cascode current mirrors and a differential pair.

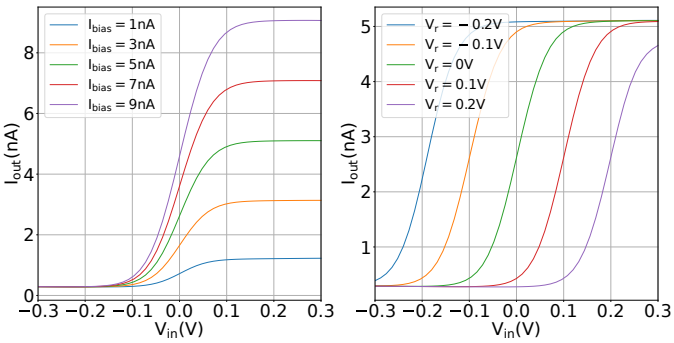

Fig. 2: The tunability in the output current via circuit parameters. The I_{bias} and V_r tunes the height and mean value respectively.

TABLE I: The sigmoid function circuit's related dimensions (Fig. 1).

NMOS	W/L (µm/µm)	PMOS	W/L (µm/µm)
M_{n1},M_{n2}	0.4/1.6	M_{p1}-M_{p6}	1.6/1.6
M_{n3}-M_{n6}	0.8/1.6	-	-

The Winner-Takes-All (WTA) circuit utilized in this study serves as an argmax operator, indicating the maximum of its inputs. Fig. 3 depicts a N_{cla}-input WTA circuit, with a constant current I_{bias} serving as the main bias point of the circuit. This configuration effectively transforms it into a current-mode comparator with multiple inputs. In this specific application, this WTA circuit assumes a crucial role in extracting the classifier's final prediction. The neuron cell with the highest input current emerges as the winner, yielding a correspondingly elevated output current. We have set all transistors' dimensions equal to $W/L = 0.4\mu m/1.6\mu m$.

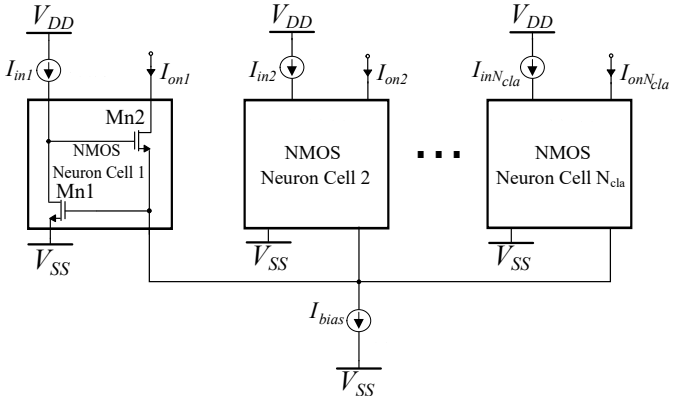

Fig. 3: A WTA circuit utilizing N_{cla} neurons based on the Standard Lazzaro NMOS architecture.

The architecture of the proposed threshold classifier is depicted in Fig. 4. Here a 2-class and N_d-feature classification problem can be solved by the implemented classifier, because it consists of a 2-neuron WTA circuit, N_d sigmoid function circuits and a threshold current. In this case only the probability of one class is calculated. Subsequently, the resulting current, which represents this probability, is compared to a predetermined threshold current by means of the WTA circuit. It is worth emphasizing that the magnitude of this threshold current significantly influences the classifier's accuracy, influencing its ability to detect true wave cases.

The proposed approach employs a combination of $N_d = 8$ univariate sigmoid function circuits for the non-linear transformation process. Each of these circuits produces an output current that signifies the likelihood of the input vector belonging to a specific class based on the corresponding feature (high or low current). Subsequently, the calculated probabilities for one class are aggregated using current mirrors (CMs), and the resulting sum is compared to a predefined threshold current, denoted as $I_{threshold}$. The classifier's prediction is conveyed through the output current I_1 of the Winner-Takes-All (WTA) circuit. This current is expressed in binary form, where a logical 1 (representing a high current value) designates the first class as the winner, while a logical 0 (indicating a low current value) signifies the second class as the winner.

IV. Software Training Co-design

To establish the required parameters for the circuit, a software-based implementation becomes essential. The datasets, available in digital format. They have undergone preprocessing to align their characteristics with the operational range of the circuit, which, in this investigation, spans from -200 to 200 mV. Subsequently, a classifier replicated in software, mirroring the number of input dimensions and classes as the equivalent hardware version, undergoes training using these datasets. Using this software-based classifier, the mean values and weights, related to each cluster, are calculated. The voltage parameter V_r and the bias currents I_{bias} are determined for the analog integrated implementation. Also, we should mention that this process is performed only once. After this procedure, the resulting parameters are subsequently exported and written in a memory (for our case analog) [15].

Each class is associated with voltage parameters $[V_{ri}]_{i=1}^{N_d}$, where N_d denotes the number of input dimensions, corresponding to the elements of the modeled sigmoid's mean vector. Also, these values can be directly written into an analog memory [15]. Each class is endowed with N_d $Ibias$ currents, which result from the multiplication of two distinct factors: the probability of each class and a normalization factor based on the training procedure. It is crucial to highlight that these bias currents are normalized within the interval of 1 to 9 nA, ensuring proper circuit functionality while keeping power consumption at a minimum.

V. Sea State or Wave Height Application and Simulation Results

In order to test the threshold classifier, a real-measurement dataset was provided by METIS Cyberspace Technology Corporation which was obtained from real-time naval vessel inertial measurements. The measurements are related to the following: Vessel hull heave displacement, Vessel hull heave speed, Vessel hull rolling angle, Vessel hull rolling turn rate, Vessel hull surge displacement, Vessel hull surge speed, Vessel hull yaw turn rate, Vessel hull pitching angle and Vessel hull pitch turn rate. This dataset comprises 40320 measurements for each of the aforementioned instances. The inertial sensors yield one measurement for each Vessel hull instance every 15 seconds. Based on a combination of papers related ML models [16] and parametric estimation of the waves [7], [9], the extracted features are the following: peak-to-peak, crest factor, root mean square, shape factor, margin factor, skewness value, impulse factor and kurtosis factor. Finally, a $70-30\%$ split was chosen for training and test sets, resulting in a total of 12096 test samples.

Here, we have evaluated the proposed classifier's performance. More specifically, concerning classification specificity and the circuit's behavior under Process, Voltage, and Temperature (PVT) variations. For this reason two separate tests are carried out on the implemented layout illustrated in Fig. 5. The total area of the layout equals $0.078mm^2$. To accommodate experimental variability, twenty different training-test iterations are performed and the related simulations results are depicted in Fig. 6. To verify the design's sensitivity a Monte Carlo analysis is performed. In particular, Fig. 7 presents the Monte Carlo Histogram. The related simulations are performed for $N = 100$ data points. The related results regarding both tests are summarized in Table II, offering a comprehensive overview of the circuit's performance and resilience. In addition, for a certain number of snapshots, we present in Fig. 8 both the height of the waves based on the measurements and whether the measurement is a wave or not. Furthermore, it also shows when the classifier makes a wrong prediction (1 False prediction) for one of the measurements.

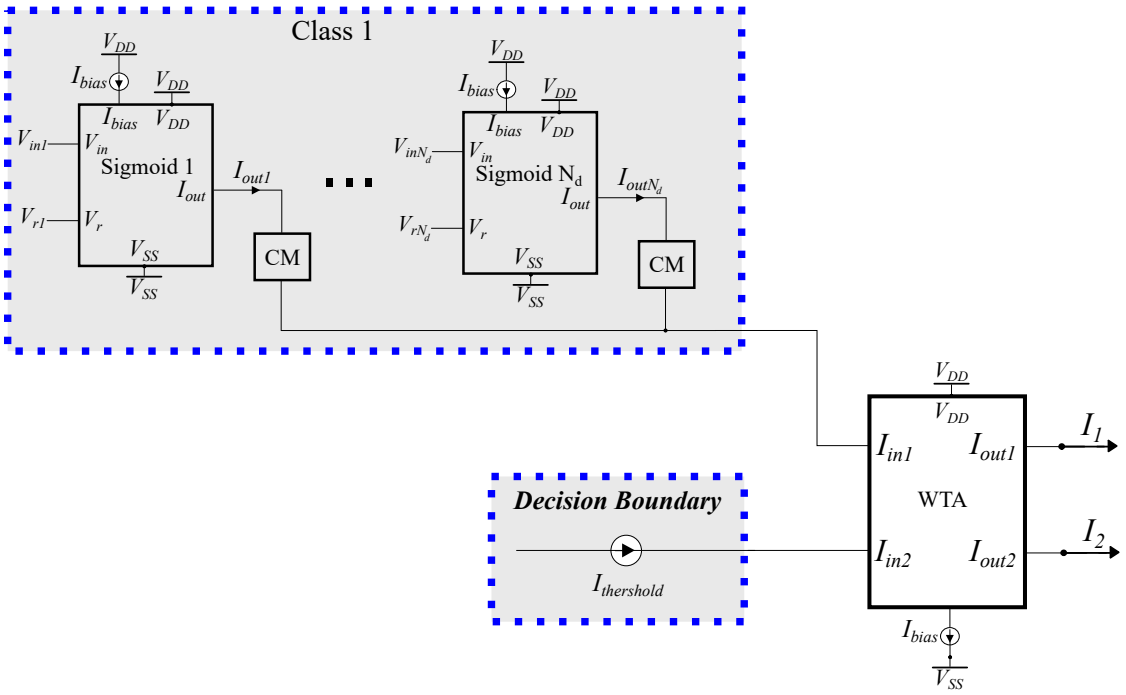

Fig. 4: The proposed classifier's top-level architecture. It consists of 2 classes and N_d features. The first class has N_d sigmoid function circuits and N_d current mirrors (CM) for the summation. The second class is a decision boundary. The WTA is used as an argmax operator.

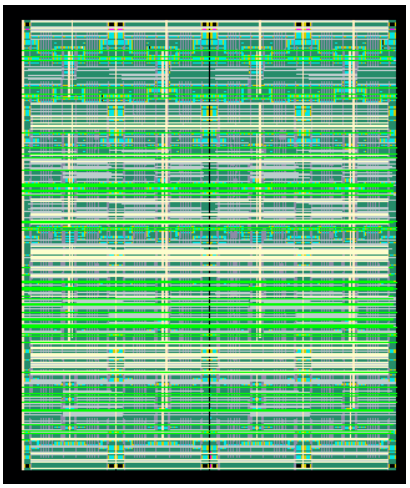

Fig. 5: The layout configuration of the proposed architecture. Also, it consists of dummy transistors.

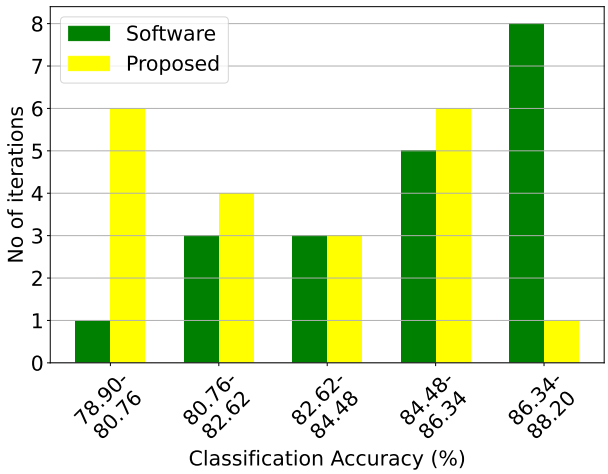

Fig. 6: Results of the implemented architecture's classification and the corresponding software model on the vessel classification dataset over twenty iterations. There is a strong correlation between the outcomes.

TABLE II: Performance Results

Method	Best	Worst	Mean	Std.
Software	88.20%	80.30%	85.50%	2.34%
Proposed	87.0%	78.90%	82.95%	2.53%
Monte Carlo	88.10%	80.50%	83.75%	1.69%

VI. Literature Summary and Performance Analysis

The literature reveals a prevalent trend where analog classifiers are often customized for particular applications. While this specificity can pose a challenge when attempting to conduct impartial comparisons across a range of implementations, it also opens up the possibility of adapting these classifiers for a shared application. This adaptation can pave the way for a thorough assessment of performance, encompassing not only ML models but also alternative methodologies. Moreover, Table III offers a comprehensive overview of our study's performance metrics alongside comparable classifiers like Multilayer Perceptron (MLP) [17], ANN [18], Long Short-Term Memory (LSTM) [19], Radial Basis function [20], K-

TABLE III: Comparison of analog classifiers on the Vessel dataset.

	Classifier	Worst accuracy	Median accuracy	Max accuracy	Power consumption	Classification speed	Energy per classification	No. of Dimensions
This work	Threshold	78.90%	82.95%	87.00%	$176nW$	$300K \frac{\text{classifications}}{\text{s}}$	$\frac{0.59 \text{ pJ}}{\text{classification}}$	8
[17]	MLP	84.60%	87.32%	91.30%	$215.14\mu W$	$930K \frac{\text{classifications}}{\text{s}}$	$\frac{231.33 \text{ pJ}}{\text{classification}}$	8
[18]	ANN	73.30%	77.42%	80.30%	$1.43\mu W$	$3M \frac{\text{classifications}}{\text{s}}$	$\frac{0.48 \text{ pJ}}{\text{classification}}$	8
[19]	LSTM	92.10%	96.13%	100.00%	$15.18mW$	$870M \frac{\text{classifications}}{\text{s}}$	$\frac{17.45 \text{ pJ}}{\text{classification}}$	8
[20]	RBF	76.70%	80.43%	82.60%	$17.95\mu W$	$200K \frac{\text{classifications}}{\text{s}}$	$\frac{89.75 \text{ pJ}}{\text{classification}}$	8
[21]	K-means	81.80%	87.33%	91.20%	$67.78\mu W$	$5M \frac{\text{classifications}}{\text{s}}$	$\frac{13.56 \text{ pJ}}{\text{classification}}$	8
[22]	Bayes	73.80%	78.67%	81.40%	$573nW$	$100K \frac{\text{classifications}}{\text{s}}$	$\frac{5.73 \text{ pJ}}{\text{classification}}$	8
[23]	Fuzzy	78.40%	82.34%	87.90%	$689nW$	$4.55K \frac{\text{classifications}}{\text{s}}$	$\frac{151.43 \text{ pJ}}{\text{classification}}$	8
[24]	Centroid	81.30%	82.45%	86.40%	$683nW$	$100K \frac{\text{classifications}}{\text{s}}$	$\frac{6.83 \text{ pJ}}{\text{classification}}$	8
[25]	GMM	77.20%	80.83%	83.60%	$612nW$	$100K \frac{\text{classifications}}{\text{s}}$	$\frac{6.12 \text{ pJ}}{\text{classification}}$	8
[26]	Threshold	78.20%	79.47%	83.90%	$312nW$	$100K \frac{\text{classifications}}{\text{s}}$	$\frac{3.12 \text{ pJ}}{\text{classification}}$	8
[27]	SVM	79.60%	80.65%	81.60%	$45.42\mu W$	$140K \frac{\text{classifications}}{\text{s}}$	$\frac{324.43 \text{ pJ}}{\text{classification}}$	8

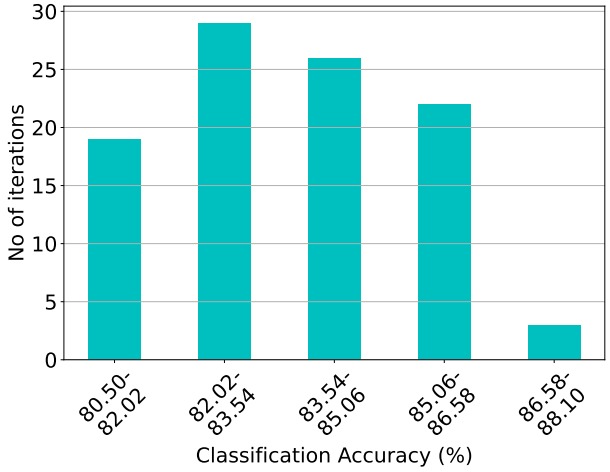

Fig. 7: Monte-Carlo simulation results after layout for the proposed architecture on the vessel classification dataset, with a mean accuracy of $\mu_M = 83.75\%$ and a standard deviation of $\sigma_M = 1.69\%$.

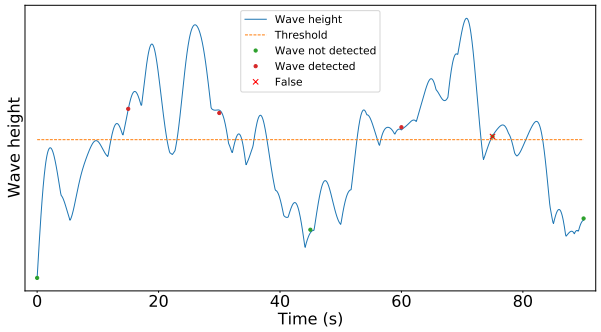

Fig. 8: Here, a specific number of snapshots related to the state of the sea are presented. They consist of wave height based on the measurements and indicate whether the measurement represents a wave or not. The inertial sensors provide a measurement every 15 seconds, and this measurement is classified (as a wave or not) by the proposed classifier. The classifier makes an incorrect prediction (False) for one of the measurements.

means [21], Bayes [22], Fuzzy [23], Centroid-based [24] Gaussian Mixture Model (GMM) [25], Gaussian Threshold [26] and Support Vector Machine (SVM) [27] all within the context of sea state or wave height application dataset.

The proposed work presents a convincing solution. It offers a balance between high accuracy, minimization of power and energy consumption per classification when compared to related works in the domain. It is essential to highlight that, in this particular application, the design does not achieve a high input dimensionality. This classifier was also tested in higher dimensionality inputs (more features classification tasks) and it gains a remarkable advantage by eliminating the necessity for Principal Component Analysis (PCA), enabling the utilization of high input dimensions. Here is necessary to achieve this without any loss of information. On the contrary, several other topologies resort to dimension reduction, limiting them to 16 dimensions, which constitutes a notable drawback in prior related works, except for the more complex models [17]–[19], [21]. As we have referred our proposed design demonstrates the capability to effectively classify multiple classes, we opt for a two-class problem to ensure a fair comparison with binary analog classifiers [23], [26], [27].

Regarding accuracy in classification, the proposed framework outperforms related literature, except for MLP [17], LSTM [19], and K-means [21]. While these implementations achieve superior accuracy, it comes at the cost of heightened complexity, increased power usage, and a larger silicon area attributable to a greater number of components. In contrast, the deployed Threshold classifier minimizes power consumption compared to alternative classifiers, presenting a balance

between accuracy and classification speed due to its simple model structure (ease of implementation). Similar findings are echoed in the Gaussian Threshold (the second-lowest power consumption) [26]. It is crucial to highlight that in applications involving inertial sensors of this nature, rapid classification speed holds less significance, mainly because of their rare incidence. As a result, in the examined design, classification speed deliberately takes a secondary role to improve accuracy and optimize/reduce power consumption. Moreover, it demonstrates lower energy consumption per classification in comparison to literature classifiers. One exception is the ANN [18]. It has a drawback that it is typical provides lower classification accuracy.

VII. Conclusion

In this study, an alternative analog integrated classifier was introduced, characterized by its ultra-low power consumption at only 176nW and its reliance on sigmoid-based thresholding. The core components of this classifier comprise circuits implementing the sigmoid function, complemented by an argmax circuit. To assess its specificity, a real-time vessel dataset was employed, with measurements taken in actual conditions. All post-layout simulations were conducted using the TSMC 90nm CMOS process, allowing for a comprehensive comparison with both software-based implementations and a diverse array of analog classifiers. Notably, the proposed implementation yielded an impressive accuracy rate of 82.95%, showcasing its potential as a fundamental component in inertial sensor systems.

VIII. Acknowledgements

This research has been co-financed by the European Union - NextGenerationEU and Greek national funds through the Greece 2.0 National Recovery and Resilience Plan, under the call RESEARCH-CREATE-INNOVATE (PROJECT CODE: TAEDK-06165). The authors would like to acknowledge METIS Cyberspace Technology Corporation for providing the data from real-time vessel measurements.

References

[1] N. El-Sheimy and A. Youssef, "Inertial sensors technologies for navigation applications: State of the art and future trends," *Satellite Navigation*, vol. 1, no. 1, pp. 1–21, 2020.

[2] J. Collin, P. Davidson, M. Kirkko-Jaakkola, and H. Leppäkoski, "Inertial sensors and their applications," *Handbook of Signal Processing Systems*, pp. 51–85, 2019.

[3] M. Kok, J. D. Hol, and T. B. Schön, "Using inertial sensors for position and orientation estimation," *arXiv preprint arXiv:1704.06053*, 2017.

[4] M. Iosa, P. Picerno, S. Paolucci, and G. Morone, "Wearable inertial sensors for human movement analysis," *Expert review of medical devices*, vol. 13, no. 7, pp. 641–659, 2016.

[5] K. Papafotis, D. Nikitas, and P. P. Sotiriadis, "Improving gyroscope's noise performance using multiple accelerometers in a closed-loop configuration," *IEEE Sensors Journal*, vol. 22, no. 22, pp. 22 062–22 068, 2022.

[6] R. W. Button, J. Kamp, T. B. Curtin, and J. Dryden, "A survey of missions for unmanned undersea vehicles," *National Defense Research Institute. RAND Corporation*, vol. 223, 2009.

[7] L. Zago, A. N. Simos, A. Kawano, and A. M. Kogishi, "A new vessel motion based method for parametric estimation of the waves encountered by the ship in a seaway," *Applied Ocean Research*, vol. 134, p. 103499, 2023.

[8] H.-M. Heyn, M. Blanke, and R. Skjetne, "Ice condition assessment using onboard accelerometers and statistical change detection," *IEEE Journal of Oceanic Engineering*, vol. 45, no. 3, pp. 898–914, 2019.

[9] U. D. Nielsen and J. Dietz, "Ocean wave spectrum estimation using measured vessel motions from an in-service container ship," *Marine Structures*, vol. 69, p. 102682, 2020.

[10] G. Xu, W. Shen, and X. Wang, "Applications of wireless sensor networks in marine environment monitoring: A survey," *Sensors*, vol. 14, no. 9, pp. 16 932–16 954, 2014.

[11] L. Parayitam, S. Sirikonda, S. Palleboina, and N. Chari, "Navigation—a general overview," *Biophysics of Insect Flight*, pp. 167–186, 2021.

[12] C. M. Bishop and N. M. Nasrabadi, *Pattern recognition and machine learning*. Springer, 2006, vol. 4, no. 4.

[13] B. Gilbert, "Translinear circuits: An historical overview," *Analog Integrated Circuits and Signal Processing*, vol. 9, pp. 95–118, 1996.

[14] J. Lazzaro, S. Ryckebusch, M. A. Mahowald, and C. A. Mead, "Winner-take-all networks of o (n) complexity," *Advances in neural information processing systems*, vol. 1, 1988.

[15] M. Hock, A. Hartel, J. Schemmel, and K. Meier, "An analog dynamic memory array for neuromorphic hardware," in *2013 European Conference on Circuit Theory and Design (ECCTD)*. IEEE, 2013, pp. 1–4.

[16] B. Panić, J. Klemenc, and M. Nagode, "Gaussian mixture model based classification revisited: Application to the bearing fault classification." *Journal of Mechanical Engineering/Strojniški Vestnik*, vol. 66, no. 4, 2020.

[17] K. Lee, J. Park, and H.-J. Yoo, "A low-power, mixed-mode neural network classifier for robust scene classification," *Journal of Semiconductor Technology and Science*, vol. 19, no. 1, pp. 129–136, 2019.

[18] S. T. Chandrasekaran, R. Hua, I. Banerjee, and A. Sanyal, "A fully-integrated analog machine learning classifier for breast cancer classification," *Electronics*, vol. 9, no. 3, p. 515, 2020.

[19] Z. Zhao, A. Srivastava, L. Peng, and Q. Chen, "Long short-term memory network design for analog computing," *ACM Journal on Emerging Technologies in Computing Systems (JETC)*, vol. 15, no. 1, pp. 1–27, 2019.

[20] S.-Y. Peng, P. E. Hasler, and D. V. Anderson, "An analog programmable multidimensional radial basis function based classifier," *IEEE Transactions on Circuits and Systems I: Regular Papers*, vol. 54, no. 10, pp. 2148–2158, 2007.

[21] R. Zhang and T. Shibata, "An analog on-line-learning k-means processor employing fully parallel self-converging circuitry," *Analog Integrated Circuits and Signal Processing*, vol. 75, pp. 267–277, 2013.

[22] V. Alimisis, G. Gennis, C. Dimas, and P. P. Sotiriadis, "An analog bayesian classifier implementation, for thyroid disease detection, based on a low-power, current-mode gaussian function circuit," in *2021 International conference on microelectronics (ICM)*. IEEE, 2021, pp. 153–156.

[23] E. Georgakilas, V. Alimisis, G. Gennis, C. Aletraris, C. Dimas, and P. P. Sotiriadis, "An ultra-low power fully-programmable analog general purpose type-2 fuzzy inference system," *AEU-International Journal of Electronics and Communications*, vol. 170, p. 154824, 2023.

[24] V. Alimisis, V. Mouzakis, G. Gennis, E. Tsouvalas, C. Dimas, and P. P. Sotiriadis, "A hand gesture recognition circuit utilizing an analog voting classifier," *Electronics*, vol. 11, no. 23, p. 3915, 2022.

[25] V. Alimisis, G. Gennis, K. Touloupas, C. Dimas, M. Gourdouparis, and P. P. Sotiriadis, "Gaussian mixture model classifier analog integrated low-power implementation with applications in fault management detection," *Microelectronics Journal*, vol. 126, p. 105510, 2022.

[26] V. Alimisis, G. Gennis, E. Tsouvalas, C. Dimas, and P. P. Sotiriadis, "An analog, low-power threshold classifier tested on a bank note authentication dataset," in *2022 International Conference on Microelectronics (ICM)*. IEEE, 2022, pp. 66–69.

[27] V. Alimisis, G. Gennis, M. Gourdouparis, C. Dimas, and P. P. Sotiriadis, "A low-power analog integrated implementation of the support vector machine algorithm with on-chip learning tested on a bearing fault application," *Sensors*, vol. 23, no. 8, p. 3978, 2023.